Charged-impurity-induced dephasing of a voltage-controlled coded qubit based on electron spin in a triple quantum dot

Puerto Gimenez, Irene; Hsieh, Chang-Yu; Korkusinski, Marek; Hawrylak, Pawel

Publisher's version / Version de l'éditeur:
https://doi.org/10.1103/PhysRevB.79.205311
Physical Review. B, Condensed Matter and Materials Physics, 79, 20, pp. 205311-1-205311-8, 2009-05-12

Charged-impurity-induced dephasing of a voltage-controlled coded qubit based on electron spin in a triple quantum dot

Irene Puerto Gimenez,[1,2] Chang-Yu Hsieh,[1] Marek Korkusinski,[1] and Pawel Hawrylak[1]
[1]*Quantum Theory Group, Institute for Microstructural Sciences, National Research Council, Ottawa, Canada K1A 0R6*
[2]*Department of Fundamental Physics, University of La Laguna, Tenerife 38205, Spain*
(Received 7 November 2008; revised manuscript received 15 April 2009; published 12 May 2009)

We discuss the effect of a charged impurity on the qubit encoded in the two low-energy states of an electrostatically defined triple quantum dot with one-electron spin in each dot. The two qubit levels are identified with the two opposite directions of the motion of a minority spin. The effect of the charged impurity on the coded qubit is mapped onto the problem of an effective spin in a random magnetic field. The effective magnetic field is related to exchange rather than Coulomb interaction which ensures stability of the coded qubit with respect to charge fluctuations.

DOI: 10.1103/PhysRevB.79.205311 PACS number(s): 73.21.La, 73.23.Hk

I. INTRODUCTION

There is currently an interest in exploiting electron spin for nanospintronic[1] and quantum information processings.[2–5] The advantages of electron-spin-based qubits are long coherence times[6] and solid-state implementation with well-established scalable semiconductor technology. In the electron-spin-based qubits described here electron spins are spatially localized in the plane of the GaAs/GaAlAs heterojunction using voltages applied to metallic gates at the GaAs surface. Due to random charge fluctuations of remote impurities[7] the confining potential may fluctuate and affect the electronic states of qubits. Hu and Das Sarma[8] studied the effect of charged impurity on two-qubit gate defined by exchange interaction between two electron-spin qubits localized in a double quantum dot. In this work we study the effect of remote charged impurity on the qubit encoded in the two low-energy levels of electrostatically defined triple quantum dot (TQD) with one-electron spin each.[9,10] A coded qubit controlled by exchange interaction composed of three spins has been proposed by Di Vincenzo *et al.*[11] Its implementation in a triple lateral quantum dot with one electron each has been proposed by some of us in Refs. 9 and 10 and a triple quantum dot molecule with controlled electron numbers has been demonstrated recently.[12,13]

In this work, starting from the microscopic model, we derive the Heisenberg Hamiltonian of a TQD in the presence of a charged impurity. We find that the charged impurity affects significantly the confining potential and the one-electron spectrum of a TQD. By contrast, the logical qubit states identified with the two opposite directions of the motion of a minority spin are coupled to charged impurity via complex exchange interactions and only weakly affected by its presence. By mapping the coded qubit into an effective two-level system, i.e., spin, the charge fluctuation translates into an effective fluctuating magnetic field. This allows us to estimate the time scale T_2^* for the charged impurity fluctuation-induced decoherence. The charge fluctuation-induced decoherence discussed here is specific to gated architecture used in creating coded qubit and is in addition to material specific individual spin decoherence mechanisms due to interaction with nuclear spins[14] and a combination of spin-orbit interaction and phonons.[15]

The paper is organized as follows. In Sec. II we present and discuss microscopic, Hubbard, and Heisenberg Hamiltonians of a coded qubit. In Sec. III we investigate the effects of the charged impurity on the electronic states of the TQD charged with one and with three electrons. In Sec. IV, we map our coded qubit into an effective spin, translate charge fluctuations into fluctuating magnetic field, and estimate a T_2^* for a model TQD device. Conclusions are given in Sec. V.

II. CODED QUBIT MODEL

A. Linear combination of harmonic-oscillator orbitals-configuration-interaction microscopic model

For our microscopic calculation, we adopt the linear combination of harmonic-oscillator orbitals-configuration-interaction (LCHO-CI) method following our previous work.[10] With energy measured in effective Rydberg and length in effective Bohr radius (see below) the dimensionless Hamiltonian of $N_{\rm el}$ electrons confined in a two-dimensional lateral TQD molecule in the presence of a charged impurity is given by

$$\hat{H}_{N\rm el} = \sum_i [-\vec{\nabla}_i^2 + V_{\rm TQD}(\vec{r}_i)] + \sum_{i<j} \frac{2}{|\vec{r}_i - \vec{r}_j|} - \sum_i \frac{2}{|\vec{r}_i - \vec{R}_{\rm imp}|}, \tag{1}$$

where $\vec{r}_i$ is the (x,y) position of ith electron, the first term is the sum of one-electron Hamiltonians $\hat{H}^o_{1\rm el}$, with $V_{\rm TQD}(\vec{r}_i)$ the TQD potential, the second term accounts for the mutual Coulomb interaction among electrons, and the third term describes interaction of electrons with charged impurity located at $\vec{R}_{\rm imp}=(R_{\rm imp}, \theta_{\rm imp}, Z_{\rm imp})$. We denote the part of Eq. (1) without the impurity term by $\hat{H}^o_{N\rm el}$. The TQD potential $V_{\rm TQD}$ is approximated by three Gaussian potentials

$$V_{\rm TQD}(\vec{r}_i) = -\sum_{k=1}^{3} V_k \exp\left(-\frac{(x_i-X_k)^2+(y_i-Y_k)^2}{d_k^2}\right). \tag{2}$$

Each Gaussian potential is characterized by depth V_k, width d_k, and center at (X_k, Y_k). With GaAs effective mass $m^*=0.067m_e$, dielectric function $\epsilon=12.4$, electron charge e, and

Planck's constant $\hbar$, the effective Rydberg is $\mathrm{Ry}^* = m^* e^4 / 2\varepsilon^2 \hbar^2 = 5.93$ meV and the effective Bohr radius is $a_B^* = \varepsilon \hbar^2 / m^* e^2 = 9.79$ nm. We consider impurity positions such that the impurity-induced potential $\frac{2}{|\vec{R}_k - \vec{R}_{\mathrm{imp}}|}$ in any dot k is much smaller than the amplitude of the electrostatically generated confinement V_k. Our theory will be illustrated by numerical results for a model TQD in GaAs with TQD parameters $V_k = 5.964$ Ry^* and $d_k = 2.41805$ a_B^* and a distance from the center of each quantum dot to the center of the structure $R_{\mathrm{TQD}} = 2.8$ a_B^*.

Following Ref. 10, the molecular single-particle states are written as linear combination of harmonic-oscillator (HO) wave functions localized at each dot (LCHO).[10] For resonant TQD with S-type HO wave function $|\phi_i\rangle$ localized at ith dot the generalized eigenvalue problem for Hamiltonian H_{1el}^o readily admits a solution in the form of Fourier transform of localized orbitals

$$|k_n\rangle = A_n \sum_{i=1}^{3} \exp\left[i\tfrac{2\pi}{3} n(i-1)\right] |\phi_i\rangle, n = -1, 0, 1,$$

$$|k_0\rangle = 1/\sqrt{3(1+2s)}(|\phi_1\rangle + |\phi_2\rangle + |\phi_3\rangle),$$

$$|k_1\rangle = 1/\sqrt{3(1-s)}(|\phi_1\rangle + e^{i2\pi/3}|\phi_2\rangle + e^{i4\pi/3}|\phi_3\rangle),$$

$$|k_{-1}\rangle = 1/\sqrt{3(1-s)}(|\phi_1\rangle + e^{-i2\pi/3}|\phi_2\rangle + e^{-i4\pi/3}|\phi_3\rangle), \quad (3)$$

where s is the overlap matrix element $\langle \phi_i | \phi_j \rangle$, $i \neq j$. The molecular ground state $|k_0\rangle$ is nondegenerate and the two excited states labeled by wave vector k, $|k_1\rangle$ and $|k_{-1}\rangle$, are degenerate and correspond to electron moving either to the left or to the right (charge current).

With states i corresponding to the molecular states $|k_i\rangle$, the properties of the N_{el} electron complex are described by the Hamiltonian written in the second-quantized form

$$\hat{H}_{N\mathrm{el}} = \sum_j \varepsilon_j^0 d_j^+ d_j + \frac{1}{2} \sum_{ijkl} \langle ji|\hat{V}|kl\rangle d_i^+ d_j^+ d_k d_l + \sum_{ij} \langle i|\hat{V}_{\mathrm{imp}}|j\rangle d_i^+ d_j, \quad (4)$$

where d_j^+ (d_j) creates (annihilates) an electron on the molecular single-particle state j (including spin) and ε_j^0 represents the corresponding single-particle energy. The first term is the sum of single-particle energies, the second sum accounts for the mutual Coulomb interaction $\langle ij|\hat{V}|kl\rangle$ among electrons, and the last sum represents the interaction $\langle i|\hat{V}_{\mathrm{imp}}|j\rangle$ between electron and the positively charged impurity.

In the subsequent discussion, we focus on a coded qubit with one electron in each quantum dot. The $S_z = -\frac{1}{2}$ subspace consists of nine configurations built with three electrons distributed on the molecular single-particle levels. In the absence of charged impurity, total wave vector $K_i = -1, 0, 1$, a sum of the wave vectors of the three molecular orbitals [Eq. (3)] of each configuration, is a good quantum number conserved in Coulomb scattering. The scattering wave vectors K's which lie outside the Brillouin zone $[-2\pi/3, 2\pi/3]$ are translated back by reciprocal-lattice vectors $(2\pi/3)n$. This reduces the 9×9, $S_z = -\frac{1}{2}$, Hamiltonian matrix written in the configuration basis $\{|K_i\rangle\}$ to a block-diagonal matrix composed of three 3×3 matrices, each of them corresponding to a value of $K = -1, 0, 1$, respectively. It follows that the eigenstates of the Hamiltonian have well defined wave vector K and can be written as a linear combination of only configurations with the same K: $|K_i^0\rangle = \Sigma_{j=1}^3 A_j^{K,i} |K_j\rangle$.

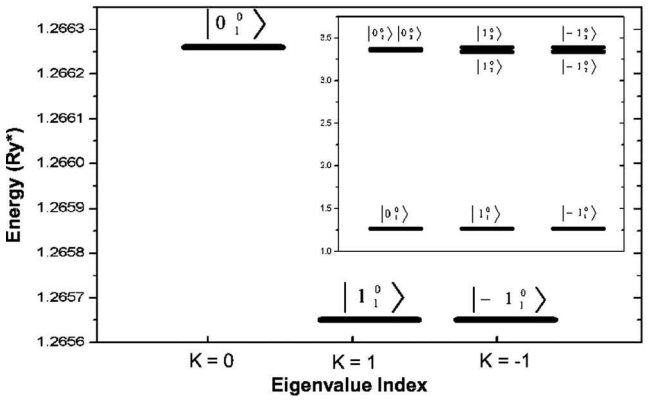

FIG. 1. The three low energy singly occupied states. The two degenerate states form a coded qubit. Inset: energy spectrum of three electrons in a resonant TQD, including singly and doubly occupied states, grouped by total $K = 0, 1, -1$.

Figure 1 shows the energy levels of the coded qubit in the absence of impurity.[9,10] The energy levels are labeled by the corresponding eigenvectors $|K_i^0\rangle$. In terms of localized configurations, the six highest levels are mostly composed of doubly occupied configurations whereas the three lowest energy levels are mainly composed of singly occupied configurations

$$|0_1^0\rangle = \frac{1}{\sqrt{3}}(c_{1\uparrow}^+ c_{2\downarrow}^+ c_{3\downarrow}^+ |0\rangle + c_{1\downarrow}^+ c_{2\uparrow}^+ c_{3\downarrow}^+ |0\rangle + c_{1\downarrow}^+ c_{2\downarrow}^+ c_{3\uparrow}^+ |0\rangle),$$

$$|1_1^0\rangle = \frac{1}{\sqrt{3}}(c_{1\uparrow}^+ c_{2\downarrow}^+ c_{3\downarrow}^+ |0\rangle + e^{i2\pi/3} c_{1\downarrow}^+ c_{2\uparrow}^+ c_{3\downarrow}^+ |0\rangle + e^{i4\pi/3} c_{1\downarrow}^+ c_{2\downarrow}^+ c_{3\uparrow}^+ |0\rangle),$$

$$|-1_1^0\rangle = \frac{1}{\sqrt{3}}(c_{1\uparrow}^+ c_{2\downarrow}^+ c_{3\downarrow}^+ |0\rangle + e^{-i2\pi/3} c_{1\downarrow}^+ c_{2\uparrow}^+ c_{3\downarrow}^+ |0\rangle + e^{i-4\pi/3} c_{1\downarrow}^+ c_{2\downarrow}^+ c_{3\uparrow}^+ |0\rangle), \quad (5)$$

where c_i^+ (c_i) creates (annihilates) an electron on the localized HO single-particle orbital i. The state $|0_1^0\rangle$ in the $K = 0$ subspace corresponds to the total spin $S = \frac{3}{2}$ while the two lowest energy coded qubit states, $|1_1^0\rangle$ and $|-1_1^0\rangle$, have $S = \frac{1}{2}$ and correspond to minority spin moving to the left or to the right and hence correspond to spin current. The two coded qubit states are separated by exchange gap Δ from the $S = \frac{3}{2}$ spin-polarized state. In our example in Fig. 1, $\Delta = 0.61$ mRy^*.

The effect of a charged impurity, the last term in Eq. (4), is to break the rotational symmetry and mix the electronic configurations belonging to different total wave vectors K. Hence the effect of impurity will be the mixing, i.e., decoherence of the two coded qubit states.

B. Hubbard and Heisenberg models

Following Ref. 16, we first establish the Hubbard Hamiltonian, including impurity potential and next derive the Heisenberg spin Hamiltonian of the coded qubit. The Hubbard model is obtained by orthogonalizing the localized HO orbitals and using them as the basis for the representation of Hamiltonian (4),

$$\hat{H}^{\mathrm{Hub}} = \sum_{\sigma}\sum_{i=1}^{3} E_i c_{i\sigma}^{+} c_{i\sigma} + \sum_{\sigma}\sum_{i\neq j} t_{ij} c_{i\sigma}^{+} c_{j\sigma} + U\sum_{i=1}^{3} n_{i\uparrow} n_{i\downarrow}. \quad (6)$$

Here E_i is the on-site energy of the ith quantum dot due to both the applied gate voltages and impurity potential, t_{ij} is the tunneling between ith and jth dots created by both gate voltages and impurity potential, U is the Coulomb repulsion between two electrons in the same dot which we here assume to be independent of the impurity, and $n_{i\sigma}=c_{i\sigma}^{+}c_{i\sigma}$ is the number operator for electrons with spin σ in ith dot. The parameters entering the Hubbard Hamiltonian can be related to the matrix elements of the one-electron Hamiltonian $\hat{H}_{1\mathrm{el}}$ and overlap matrix elements

$$\begin{aligned} E_i &= \langle\phi_i|\hat{H}_{1\mathrm{el}}|\phi_i\rangle + 2\tilde{s}(\langle\phi_i|\hat{H}_{1\mathrm{el}}|\phi_j\rangle + \langle\phi_i|\hat{H}_{1\mathrm{el}}|\phi_k\rangle) \\ &\quad + \tilde{s}^2(\langle\phi_j|\hat{H}_{1\mathrm{el}}|\phi_j\rangle + \langle\phi_k|\hat{H}_{1\mathrm{el}}|\phi_k\rangle + 2\langle\phi_j|\hat{H}_{1\mathrm{el}}|\phi_k\rangle), \\ t_{ij} &= \langle\phi_i|\hat{H}_{1\mathrm{el}}|\phi_j\rangle + \tilde{s}(\langle\phi_i|\hat{H}_{1\mathrm{el}}|\phi_i\rangle + \langle\phi_j|\hat{H}_{1\mathrm{el}}|\phi_j\rangle + \langle\phi_i|\hat{H}_{1\mathrm{el}}|\phi_k\rangle \\ &\quad + \langle\phi_j|\hat{H}_{1\mathrm{el}}|\phi_k\rangle) + \tilde{s}^2(\langle\phi_k|\hat{H}_{1\mathrm{el}}|\phi_k\rangle + \langle\phi_i|\hat{H}_{1\mathrm{el}}|\phi_j\rangle \\ &\quad + \langle\phi_i|\hat{H}_{1\mathrm{el}}|\phi_k\rangle + \langle\phi_j|\hat{H}_{1\mathrm{el}}|\phi_k\rangle), \end{aligned} \quad (7)$$

where $\tilde{s}=\frac{1}{3}\left(\frac{1}{\sqrt{1+2s}}-\frac{1}{\sqrt{1-s}}\right)$ is defined with respect to localized HO orbital overlap matrix elements s.

Next, we map the low-energy spectrum of the Hubbard Hamiltonian into the Heisenberg Hamiltonian

$$\hat{H}^{\mathrm{Heis}} = \sum_{i<j} J_{ij}\vec{S}_i\cdot\vec{S}_j. \quad (8)$$

The Heisenberg Hamiltonian yields the coded qubit states obtained via the LCHO-CI method. We compute the exchange constants J_{ij} from the Hubbard Hamiltonian (6) through perturbation theory in strong Coulomb interaction regime ($U\gg t_{ij}$). We find

$$J_{ij} = 4\frac{(t_{ij})^2}{U}\left(\frac{2}{1-(\Delta E_{ij}/U)^2}\right), \quad (9)$$

where $\Delta E_{ij}=E_i-E_j$. In the absence of impurity all quantum dot energies E_i are equal and hence all exchange constants are equal. The presence of impurity leads to modifications of both energy levels E_i and tunneling matrix elements t_{ij}, and hence leads to different exchange interactions J_{ij} for different pairs of spins i and j. The changes in J_{ij} depend on the ratio of the impurity-induced difference in dot energies ΔE_{ij} to the on-site Coulomb repulsion U.

III. EFFECT OF IMPURITY ON A CODED QUBIT

A. Effect of impurity on the one-electron spectrum

We now analyze the effect of a charged impurity, the last term in Eq. (4), on the one-electron spectrum. We only consider impurity positions which weakly modify the confining potential of the resonant TQD.

After some algebra, the one-electron Hamiltonian, written in the basis of molecular states $\{|k_0\rangle,|k_1\rangle,|k_{-1}\rangle\}$, reads

$$H_{1\mathrm{el}} = \begin{pmatrix} \varepsilon_{k_0}^0 + C_{00}^{\mathrm{ov}}(\bar{E}_{\mathrm{imp}} + 2\bar{t}_{\mathrm{imp}}) & C_{01}^{\mathrm{ov}}(\widetilde{\delta E}_{\mathrm{imp}} - \widetilde{\delta t}_{\mathrm{imp}}) & C_{01}^{\mathrm{ov}}(\widetilde{\delta E}_{\mathrm{imp}} - \widetilde{\delta t}_{\mathrm{imp}})^* \\ C_{01}^{\mathrm{ov}}(\widetilde{\delta E}_{\mathrm{imp}} - \widetilde{\delta t}_{\mathrm{imp}})^* & \varepsilon_{k_{-1}}^0 + C_{11}^{\mathrm{ov}}(\bar{E}_{\mathrm{imp}} - \bar{t}_{\mathrm{imp}}) & C_{11}^{\mathrm{ov}}(\widetilde{\delta E}_{\mathrm{imp}} + 2\widetilde{\delta t}_{\mathrm{imp}}) \\ C_{01}^{\mathrm{ov}}(\widetilde{\delta E}_{\mathrm{imp}} - \widetilde{\delta t}_{\mathrm{imp}}) & C_{11}^{\mathrm{ov}}(\widetilde{\delta E}_{\mathrm{imp}} + 2\widetilde{\delta t}_{\mathrm{imp}})^* & \varepsilon_{k_{+1}}^0 + C_{11}^{\mathrm{ov}}(\bar{E}_{\mathrm{imp}} - \bar{t}_{\mathrm{imp}}) \end{pmatrix}. \quad (10)$$

The first terms in the diagonal, $\varepsilon_{k_n}^0, n=0,-1,1$, give the energy of the molecular ground state $|k_0\rangle$ and two degenerate excited states $|k_{-1}\rangle,|k_{+1}\rangle$, respectively. All remaining terms correspond to impurity effects. Here $\bar{E}_{\mathrm{imp}}=\frac{1}{3}\Sigma_{j=1}^{3}E_j^{\mathrm{imp}}$ is the average shift of the energy levels due to impurity with $E_j^{\mathrm{imp}}=\langle\phi_j|\hat{V}_{\mathrm{imp}}|\phi_j\rangle$. $\bar{t}_{\mathrm{imp}}=\frac{1}{3}\Sigma_{i<j=1}^{3}t_{ij}^{\mathrm{imp}}, i\neq j$ is the average shift of the tunneling matrix elements due to impurity, with $t_{ij}^{\mathrm{imp}}=\langle\phi_i|\hat{V}_{\mathrm{imp}}|\phi_j\rangle$. $\widetilde{\delta E}_{\mathrm{imp}}=\frac{1}{3}\Sigma_{j=1}^{3}\delta E_j^{\mathrm{imp}}e^{i2\pi/3(j-1)}$ is related to a shift in quantum dot energy measured from the average shift due to impurity $\delta E_i^{\mathrm{imp}}=E_i^{\mathrm{imp}}-\bar{E}_{\mathrm{imp}}$ and $\widetilde{\delta t}_{\mathrm{imp}}=\frac{1}{3}(\delta t_{23}^{\mathrm{imp}}+\delta t_{13}^{\mathrm{imp}}e^{i2\pi/3}+\delta t_{12}^{\mathrm{imp}}e^{i4\pi/3})$ depends on deviation of each tunneling matrix element from their average $\delta t_{ij}^{\mathrm{imp}}=t_{ij}^{\mathrm{imp}}-\bar{t}_{\mathrm{imp}}, i\neq j$. Coefficients $C_{00}^{\mathrm{ov}}=\frac{1}{(1+2s)}$, $C_{01}^{\mathrm{ov}}=\frac{1}{\sqrt{1-s}\sqrt{1+2s}}$, and $C_{11}^{\mathrm{ov}}=\frac{1}{(1-s)}$, with $s=\langle\phi_i|\phi_j\rangle, i\neq j$, account for the nonorthogonality of the HO basis.

The effect of impurity potential on the one-electron spectrum is illustrated in Fig. 2 for a charged impurity located at $R_{\mathrm{imp}}=3R_{\mathrm{TQD}}$, $\theta_{\mathrm{imp}}=\pi/3$, and $Z_{\mathrm{imp}}=4R_{\mathrm{TQD}}$. We start on the left of Fig. 2 with the one-electron spectrum in the absence of impurity. We first consider the effect E_{imp} of impurity on on-site energy levels shown as the second column in Fig. 2. In the third column, we turn on the effect t_{imp} of impurity on interdot tunneling. We see that these effects of impurity are

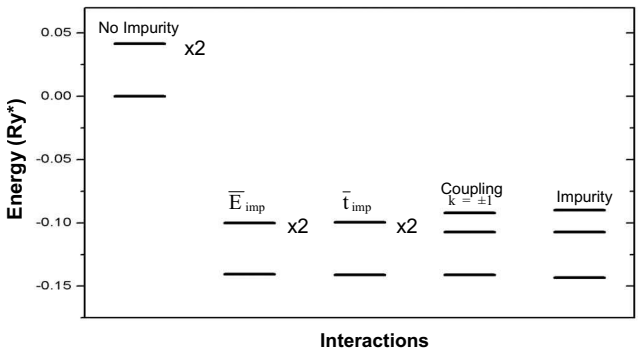

FIG. 2. Evolution of the energy levels of one electron in a triple quantum dot in the presence of a charged impurity as function of interaction type. See text for details. "x2" denotes a doubly degenerate level.

to lower the energy of all levels proportional to the average impurity shift $\bar{E}_{\mathrm{imp}}$ and increase the energy gap between ground and excited states by 3 times the average impurity-induced tunneling matrix element, $3\bar{t}_{\mathrm{imp}}$. In our numerical example this shift is small due to the small overlaps between localized orbitals ($s=2.64\times10^{-3}$).

Next we consider the coupling of states $|k_1\rangle$ and $|k_{-1}\rangle$ caused by the impurity potential in the fourth column of Fig. 2. The energy gap is given by $\Delta\varepsilon_{\mathrm{GAP}}^{\mathrm{1el}}=2|C_{11}^{\mathrm{ov}}(\widetilde{\delta E}_{\mathrm{imp}}+2\widetilde{\delta t}_{\mathrm{imp}})|$. Due to the small overlaps, i.e., $\delta t_{ij}^{\mathrm{imp}}\approx10^{-3}\delta E_i^{\mathrm{imp}}$, the energy gap created by impurity can be approximated by

$$\Delta\varepsilon_{\mathrm{GAP}}^{\mathrm{1el}}\approx 2|\widetilde{\delta E}_{\mathrm{imp}}| = \frac{2}{3}\sqrt{\left(E_1^{\mathrm{imp}}-\frac{E_2^{\mathrm{imp}}+E_3^{\mathrm{imp}}}{2}\right)^2+\frac{3}{4}(E_2^{\mathrm{imp}}-E_3^{\mathrm{imp}})^2}. \tag{11}$$

If we neglect the coupling of the excited states to the $|k_0\rangle$ state which has much lower energy, we conclude that the energy gap caused by the impurity is proportional to the differences between the impurity on-site shifts $E_i^{\mathrm{imp}}=\langle\phi_i|\frac{-2}{|\vec{r}-\vec{R}_{\mathrm{imp}}|}|\phi_i\rangle$. Making a Taylor-series expansion and keeping only the first term we find that the energy shift due to the impurity potential of dot i is $E_i^{\mathrm{imp}}\approx\frac{-2}{|\vec{R}_i-\vec{R}_{\mathrm{imp}}|}$, where $\vec{R}_i$ is the position of the center of dot i. Therefore the energy gap created by the impurity is proportional to the differences between the values of the impurity potential at the center of each dot. In the last two columns of Fig. 2 we compare the approximate gap to the gap calculated by exact diagonalization and we see that the two approaches agree very well.

Figure 3 shows the one-electron spectra of the TQD as a function of impurity positions calculated by diagonalization of the Hamiltonian (4) with $N_{\mathrm{el}}=1$. The spectra show the splitting of the doubly degenerate levels, its dependence on the distance of the impurity from the TQD, and on the position with respect to symmetry axis of the TQD. The charged impurity modifies the one-electron spectra through direct Coulomb interaction, which mixes states $|k_1\rangle$ and $|k_{-1}\rangle$ and redistributes charge density on the dots as a function of charged impurity positions. Hence, results from Fig. 3 indicate that any quantum information processing schemes trying to utilize the electron's charge degree of freedom[17,18] will have to consider the decoherence channel induced by the charge fluctuations.

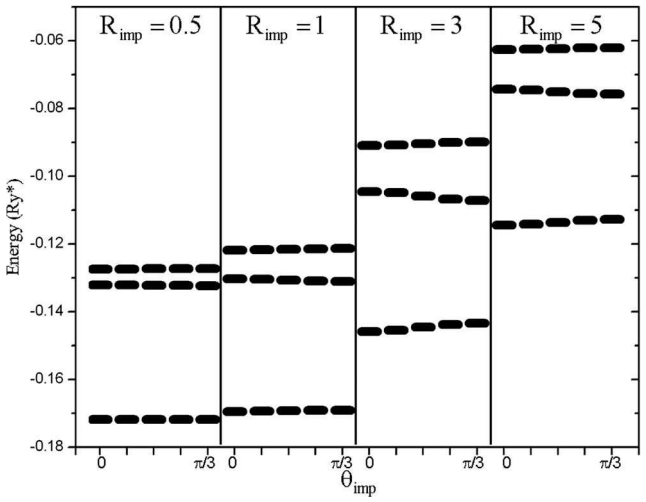

FIG. 3. Energy spectrum of one electron in a TQD in the presence of an impurity located in the plane $Z_{\mathrm{imp}}=4R_{\mathrm{TQD}}$ as a function of R_{imp} and θ_{imp}. R_{imp} is given in units of R_{TQD}. θ_{imp} is measured from the symmetry axis that goes through the center of a quantum dot. The zero energy is set to the ground level of the resonant TQD.

B. Effect of impurity on the coded qubit spectrum

We calculate the eigenenergies and eigenvectors of the coded qubit Hamiltonian in the presence of impurity (4) in the basis of eigenvectors of the resonant TQD with three electrons without the impurity, $\{|K_i^0\rangle\}$, discussed in Sec. II. The impurity matrix elements in the basis $\{|K_i^0\rangle\}$ are calculated as a linear combination of the impurity matrix elements in the basis of configurations $\{|K_i\rangle\}$,

$$\langle K_i^0|\hat{V}_{\mathrm{imp}}|K_j'^0\rangle=\sum_{p=1}^{3}\sum_{q=1}^{3}A_p^{K,i}A_q^{K',j}\langle K_p|\hat{V}_{\mathrm{imp}}|K_q'\rangle, \tag{12}$$

with

$$\langle K_p|\hat{V}_{\mathrm{imp}}|K_q'\rangle=\langle 0|d_{k_{p3\uparrow}}d_{k_{p2\downarrow}}d_{k_{p1\downarrow}}\left|\sum_{n=-1}^{1}\sum_{m=-1}^{1}\tilde{V}_{\mathrm{nm}}^{\mathrm{imp}}d_{k_n}^{+}d_{k_m}\right| \times d_{k_{q1\downarrow}}^{+}d_{k_{q2\downarrow}}^{+}d_{k_{q3\uparrow}}^{+}|0\rangle,$$

which is zero unless configurations $|K_p\rangle$ and $|K_q'\rangle$ differ at most in the spin orbital of only one of the three electrons. $A_p^{K,i}$ are the coefficients of the three-electron eigenfunctions $\{|K_i^0\rangle\}$ written in terms of the configurations $\{|K_i\rangle\}$ and $\tilde{V}_{\mathrm{nm}}^{\mathrm{imp}}=\langle k_n|\frac{-2}{|\vec{r}-\vec{R}_{\mathrm{imp}}|}|k_m\rangle$ are the molecular impurity matrix elements.

Figure 4(a) shows the splitting of low-energy levels (black lines) of a coded qubit obtained by the diagonalization of the full Hamiltonian for various distances between the TQD and the charged impurity. Figure 4(b) shows the same splitting but as a function of the positions with respect to symmetry axis of the TQD.

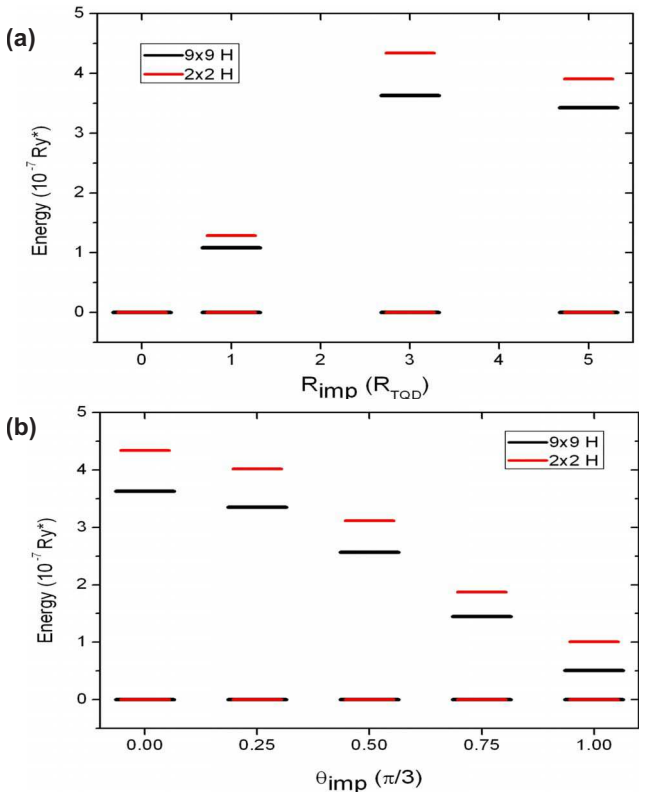

FIG. 4. (Color online) Two lowest energy levels of three electrons in a TQD in the presence of an impurity for different impurity positions in the plane $Z_{\text{imp}}=4R_{\text{TQD}}$, with ground level normalized to zero. Top: radius dependence for $\theta_{\text{imp}}=0$. Bottom: angle dependence for impurity $R_{\text{imp}}=3R_{\text{TQD}}$.

The full Hamiltonian containing all doubly and singly occupied configurations can be approximated by the 2×2 Hamiltonian in the subspace of the two logical qubit levels $|1_1^0\rangle$ and $|-1_1^0\rangle$. The spectra obtained by diagonalizing this approximate 2×2 Hamiltonian, shown as shorter lines in Fig. 4, agree well with results of the full calculations.

Let us now turn to the analysis of the effects of charged impurity on the coded qubit described by the Heisenberg model. For a system of three localized spins with total $S_z=-\frac{1}{2}$ we can build a basis equivalent to the eigenvectors of Eq. (5), in terms of states describing minority spin moving to the left, to the right, or being stationary, as

$$\{|K^{\text{Heis}}\rangle\}=\Big\{|1^{\text{Heis}}\rangle=\tfrac{1}{\sqrt{3}}(|\uparrow\downarrow\downarrow\rangle+e^{i2\pi/3}|\downarrow\uparrow\downarrow\rangle+e^{i4\pi/3}|\downarrow\downarrow\uparrow\rangle),$$

$$|-1^{\text{Heis}}\rangle=\tfrac{1}{\sqrt{3}}(|\uparrow\downarrow\downarrow\rangle+e^{-i2\pi/3}|\downarrow\uparrow\downarrow\rangle+e^{-i4\pi/3}|\downarrow\downarrow\uparrow\rangle),$$

$$|0^{\text{Heis}}\rangle=\tfrac{1}{\sqrt{3}}(|\uparrow\downarrow\downarrow\rangle+|\downarrow\uparrow\downarrow\rangle+|\downarrow\downarrow\uparrow\rangle)\Big\}.$$

After some algebra, the Heisenberg Hamiltonian in this basis reads

$$H^{\text{Heis}}=\begin{bmatrix}-3/4J_{\text{av}} & 3/2\Delta^* & 0\\ 3/2\Delta & -3/4J_{\text{av}} & 0\\ 0 & 0 & 3/4J_{\text{av}}\end{bmatrix}, \tag{13}$$

where $J_{\text{av}}=\frac{J_{12}+J_{13}+J_{23}}{3}$, $\Delta=\frac{J_{23}+e^{i2\pi/3}J_{12}+e^{i4\pi/3}J_{13}}{3}$, and the exchange couplings are positive. Similarly to $|0_1^0\rangle$ in Eq. (5), the basis vector $|0^{\text{Heis}}\rangle$ has $S=\frac{3}{2}$ and does not couple to the $S=\frac{1}{2}$ vectors $|1^{\text{Heis}}\rangle$ and $|-1^{\text{Heis}}\rangle$, which form the spin-coded qubit. For a resonant TQD these two qubit states are degenerate, J's are equal and $|\Delta|=0$, reproducing the results of microscopic calculations. When the system is detuned by the charged impurity the coded qubit levels are mixed and split, with the energy gap given by

$$\Delta\varepsilon_{\text{GAP}}^{\text{3el}}=3|\Delta|=\sqrt{\left(J_{23}-\frac{J_{12}+J_{13}}{2}\right)^2+\frac{3}{4}(J_{12}-J_{13})^2}. \tag{14}$$

We see that the energy gap in the three-electron TQD created by the impurity depends on differences in J_{ij}, which depend on $(t_{ij})^2$ and ΔE_{ij} through Eq. (9). For a resonant TQD, neglecting the dependence of tunneling matrix elements on impurity potential allows us to express the gap in the coded qubit spectrum in terms of the exchange constant in the absence of impurity, J_0, and $(\Delta E_{ij}/U)^2$,

$$\Delta\varepsilon_{\text{GAP}}^{\text{3el}}=J_0\sqrt{\left[(\Delta E_{23}/U)^2-\frac{(\Delta E_{12}/U)^2+(\Delta E_{13}/U)^2}{2}\right]^2+\frac{3}{4}[(\Delta E_{12}/U)^2-(\Delta E_{13}/U)^2]^2}. \tag{15}$$

We see that while the splitting of the single-particle spectrum is proportional to differences of single-particle energies ΔE_{ij}, the splitting of coded qubit levels is proportional to differences in $(\Delta E_{ij}/U)^2$. Since $\Delta E_{ij}\ll U$, the energy gap created by the impurity in the three-electron spectrum is several orders of magnitude smaller than the gap created in the one-electron spectrum. In other words, the direct Coulomb repulsion significantly modifies the charge distribution of the TQD in single electron case. In the case of three highly localized electrons, the effect of charged impurity is to modify the spin distribution of the TQD through much weaker exchange interactions.

IV. DEPHASING OF THE CODED QUBIT

A. Effective random magnetic fields

It has been shown in Sec II A that the two eigenstates of the degenerate ground state of three electrons with $S_z=-\frac{1}{2}$ in

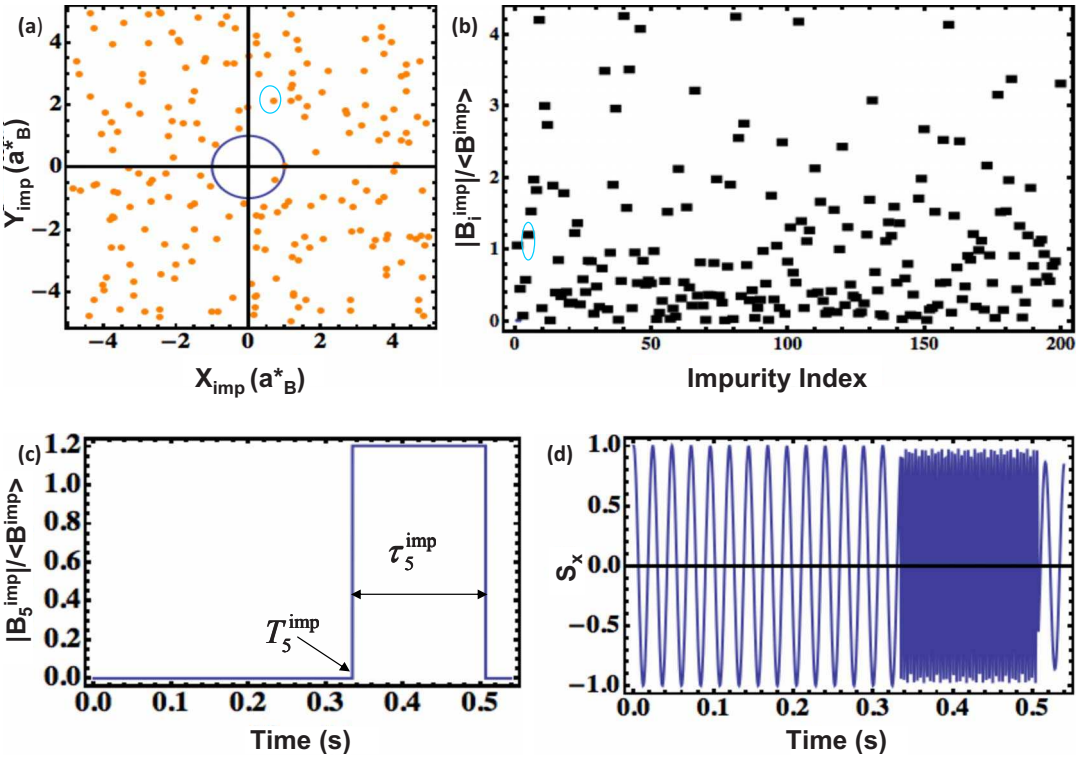

FIG. 5. (Color online) Top left: the x and y coordinates of 200 charged impurities randomly generated in a rectangular box restricted in x, y, and z dimensions from -5 R_{TQD} to 5 R_{TQD}, from -5 R_{TQD} to 5 R_{TQD}, and from 4 R_{TQD} to 8 R_{TQD}, respectively. Circle of radius 1 R_{TQD} around the origin outlines the size of the TQD device while the center of the TQD is located at the origin. The circled impurity is used in experiment no. 5. Top right: The magnitudes of effective magnetic fields due to 200 charged impurities in the ensemble. The circled effective magnetic field is used in experiment no. 5. Lower left: the fluctuation of the effective magnetic field in experiment no. 5 is specified by T_5^{imp}, the time it is switched on, and τ_5^{imp}, its lifetime. Lower right: the simulated time evolution of x component of Bloch vector, $S_x(t)$, in effective magnetic field $\mathbf{B}^{\mathrm{ext}}+\mathbf{B}_5^{\mathrm{imp}}$, for experiment no. 5. In this study, we set $\mathbf{B}^{\mathrm{ext}}=\langle\mathbf{B}^{\mathrm{imp}}\rangle$.

a triple quantum dot, $|1_1^0\rangle$ and $|-1_1^0\rangle$, form a coded qubit. State $|0_L\rangle=|1_1^0\rangle$ is identified with minority spin moving clockwise and state $|1_L\rangle=|-1_1^0\rangle$ with minority spin moving anticlockwise. Initialization of the qubit states is possible by applying a magnetic field perpendicular to the TQD.[19] In Sec. III B we showed that the effect of the impurity on this qubit can be described by the effective 2×2 Hamiltonian

$$\hat{H}^{\mathrm{qubit}}=\begin{pmatrix} E_o+\langle 0_L|\hat{V}_{\mathrm{imp}}|0_L\rangle & \langle 0_L|\hat{V}_{\mathrm{imp}}|1_L\rangle \\ \langle 1_L|\hat{V}_{\mathrm{imp}}|0_L\rangle & E_o+\langle 1_L|\hat{V}_{\mathrm{imp}}|1_L\rangle \end{pmatrix}, \quad (16)$$

where E_o is the energy of the qubit level in the absence of impurity and the impurity matrix elements are calculated with Eq. (12). Hence the coded qubit is an effective spin $S=\frac{1}{2}$ with clockwise spin-current state $|0_L\rangle$ corresponding to spin up and counterclockwise spin-current state $|1_L\rangle$ represented by spin down. In this picture the charged impurity acts as an effective magnetic field $\vec{B}^{\mathrm{eff}}$. Since charge densities of both qubit states are equal, the impurity couples to each of them in the same manner, hence $\langle 0_L|\hat{V}_{\mathrm{imp}}|0_L\rangle=\langle 1_L|\hat{V}_{\mathrm{imp}}|1_L\rangle$. It follows that the impurity effective magnetic field $\vec{B}^{\mathrm{eff}}$ does not have a z component. The in-plane component of $\vec{B}^{\mathrm{eff}}$ $\approx\langle 0_L|\hat{V}_{\mathrm{imp}}|1_L\rangle$ flips the spin and leads to dephasing of the coded qubit. We have converted the charged impurity-induced decoherence problem to a problem of dephasing of a spin by a random magnetic field.[20–22] We have shown how to compute this effective field once the fluctuating impurity is identified.

B. Estimation of T_2^*

We now turn to estimate T_2^* of the coded qubit due to the fluctuating in-plane magnetic field.[20,21] Following Ref. 7, on average, we expect each charged impurity to last 1.0 s with a quiet interval of 0.2 s between successive impurity appearances. These experimental findings suggest that there is a significant mismatch between charged impurity fluctuating time scale and inherent coded qubit dynamics time scale, which is characterized by $\Delta\epsilon_{\mathrm{GAP}}^{3\mathrm{el}}/\hbar=O(\mu s)$. Hence we only need to simulate the time evolution of the coded qubit in the presence of a single charged impurity. First, we initialize a coded qubit at $t=0$ in a given state. Next, we randomly select position of impurity, its switch-on time T^{imp}, and lifetime τ^{imp}. We then simulate the time evolution of the coded qubit up to certain time t^* and measure its state. This constitutes one complete numerical experiment in our study. We repeat the same procedures N times; each time we initialize the coded qubit in exactly the same state but let it evolve in the presence of different charged impurity. The averaged time evolution, based on these N numerical experiments, of the

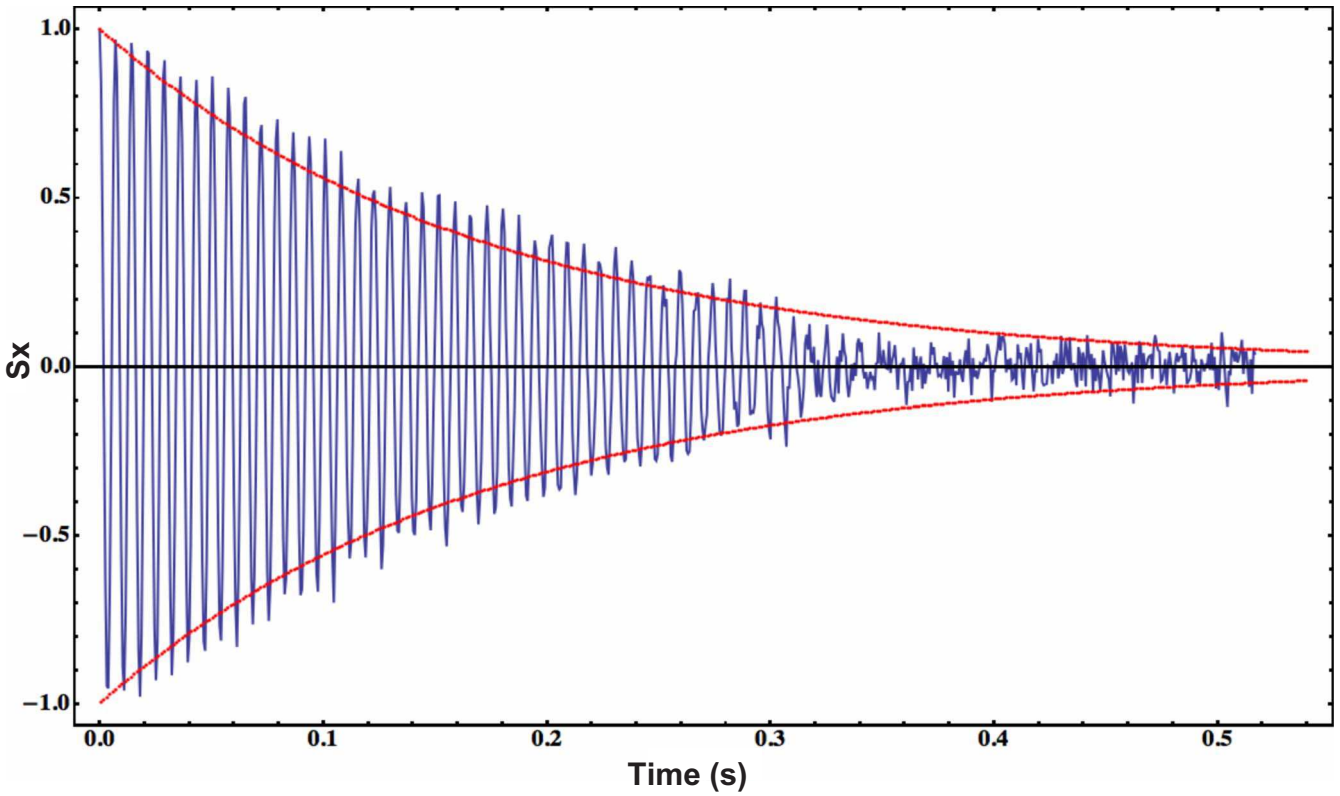

FIG. 6. (Color online) Oscillating curve represents the simulated time evolution of the averaged Bloch vector x component, $<S_x(t)>$. Decaying curve shows the envelope of the decaying oscillation for the x component of effective Bloch vector, $S_{\mathrm{eff},x}(t)$.

off-diagonal density-matrix elements of the coded qubit suffers exponential decay, which is characterized by T_2^*.

Figure 5(a) shows the positions of $N=200$ randomly generated charged impurities used in this study. For each of these 200 charged impurities, we perform LCHO-CI calculation to obtain the effective magnetic field as explained in Sec. IV A. Figure 5(b) shows the distribution of effective magnetic fields. Next, we specify the fluctuating aspects of the effective magnetic field by assigning the lifetime τ_i^{imp} and switch-on time T_i^{imp} to the ith charged impurity. The random generations of τ_i^{imp} and T_i^{imp} are done with the mean of the distribution equal to 1.0 and 0.2 s as extracted from Ref. 7.

At this stage, we have completely specified the fluctuating magnetic fields due to charged impurities. We next solve the Bloch equation of the coded qubit separately for each experiment,

$$\frac{d\mathbf{S}_i}{dt} = \gamma \mathbf{S}_i \times (\mathbf{B}_i^{\mathrm{imp}}(t) + \mathbf{B}^{\mathrm{ext}}), \tag{17}$$

where $S_x=\rho_{12}+\rho_{21}$, $S_y=i(\rho_{12}-\rho_{21})$, and $S_z=\rho_{22}-\rho_{11}$, ρ_{ij} are density-matrix elements of the coded qubit, $\mathbf{B}_i^{\mathrm{imp}}(t)$ is the effective magnetic field due to ith impurity, $\mathbf{B}^{\mathrm{ext}}$ denotes the effective external magnetic field, and γ is effective gyromagnetic ratio of the coded qubit inferred from $\gamma|\mathbf{B}_i^{\mathrm{imp}}(t)|\hbar = \Delta\epsilon_{\mathrm{GAP}}^{3\mathrm{el}}$. Let us follow through the entire computational procedure for one particular impurity. In Figs. 5(a) and 5(b), a circle is drawn, respectively, around the charged impurity position no. 5 and the associated effective magnetic field derived from LCHO-CI calculation. Figure 5(c) shows the $\mathbf{B}_5^{\mathrm{imp}}$, which is turned on at T_5^{imp} and lasts for τ_5^{imp}. Figure 5(d) shows the time evolution of Bloch vector component $S_x(t)$ for the coded qubit in the presence of $\mathbf{B}^{\mathrm{ext}}+\mathbf{B}_5^{\mathrm{imp}}$ and $\mathbf{B}^{\mathrm{ext}} = \langle \mathbf{B}^{\mathrm{imp}} \rangle = \Sigma_i \mathbf{B}_i^{\mathrm{imp}}(t)/N$. As shown in the figure, the coded qubit always undergoes coherent time evolution even in the presence of charge fluctuations. The dephasing of Bloch vector, similar to inhomogeneous broadening effects in NMR characterized by T_2^*, only emerges from averaging the time evolutions of the coded qubit over N impurities, i.e., $\langle \mathbf{S}(\mathbf{t}) \rangle = \Sigma_i \mathbf{S}_i(t)/N$.

To estimate T_2^*, we fit $\langle \mathbf{S}(\mathbf{t}) \rangle$ to the result of the time evolution of $\mathbf{S}_{\mathrm{eff}}$ satisfying effective Bloch equation with parameter T_2^*,

$$\frac{d\mathbf{S}_{\mathrm{eff}}}{dt} = \gamma \mathbf{S}_{\mathrm{eff}} \times \mathbf{B}^{\mathrm{ext}} - \frac{\mathbf{S}_{\mathrm{eff},\perp}}{T_2^*}, \tag{18}$$

where $\mathbf{S}_{\mathrm{eff}}$ denotes the effective Bloch vector and $\mathbf{S}_{\mathrm{eff},\perp}$ denotes the effective Bloch vector perpendicular to the externally applied field. The value of T_2^* is a function of $\langle T^{\mathrm{imp}} \rangle$, $\langle \tau^{\mathrm{imp}} \rangle$, and averaged distance of the charged impurity from the TQD with dominant contribution from $\langle T^{\mathrm{imp}} \rangle$.

Figure 6 shows the simulated and fitted result of $\langle S_x(t) \rangle$ in the presence of external field $\mathbf{B}^{\mathrm{ext}}=\langle \mathbf{B}^{\mathrm{imp}} \rangle$, with extracted value $T_2^*=0.2s$. These times are much longer than the reported dephasing times of individual spins due to nuclear spins.[21,23,24]

V. CONCLUSIONS

In conclusion, we discussed here the effects of a charged impurity on the qubit encoded in the two low-energy levels of an electrostatically defined triple quantum dot with one-electron spin in each dot. The two qubit levels were identified with the two opposite directions of the motion of a minority spin. The effects of the random charged impurity on the coded qubit were mapped onto the problem of an effective spin in a random magnetic field. The effective magnetic field was computed as a function of impurity position. It was shown that the effective magnetic field is related to variations of exchange interaction, which were demonstrated to be orders of magnitude smaller than the impurity-induced variations of the one-electron levels. These results predict stability of the coded qubit based on electron spin with respect to random charge fluctuations. We estimate the inhomogeneous dephasing time T_2^* of coded qubit and find it to be much longer than the dephasing times due to nuclear spins.

ACKNOWLEDGMENTS

The authors thank F. Delgado, Y.-P. Shim, and A. Sachrajda for discussions. The authors are grateful to the Canadian Institute for Advanced Research, QuantumWorks, and NSERC for support. I.P.G. acknowledges financial supports of Spanish Ministerio de Educación y Ciencia under Grant No. AP-2004-0143 and Plan Nacional under Grant No. FIS-2007-64018.

[1] A. Sachrajda, P. Hawrylak, and M. Ciorga, in *Electronic Transport in Quantum Dots*, edited by J. P. Bird (Kluwer Academic, Boston, 2003).
[2] J. A. Brum and P. Hawrylak, Superlattices Microstruct. **22**, 431 (1997).
[3] M. Korkusinski and P. Hawrylak, in *Semiconductor Quantum Bits*, edited by O. Benson and F. Henneberger (World Scientific, Singapore, 2008).
[4] D. Loss and D. P. DiVincenzo, Phys. Rev. A **57**, 120 (1998).
[5] R. Hanson, L. Kouwenhoven, J. Petta, S. Tarucha, and L. Vandersypen, Rev. Mod. Phys. **79**, 1217 (2007).
[6] R. Hanson, B. Witkamp, L. M. K. Vandersypen, L. H. Willems van Beveren, J. M. Elzerman, and L. P. Kouwenhoven, Phys. Rev. Lett. **91**, 196802 (2003).
[7] M. Pioro-Ladriere, J. H. Davies, A. R. Long, A. S. Sachrajda, L. Gaudreau, P. Zawadzki, J. Lapointe, J. Gupta, Z. Wasilewski, and S. Studenikin, Phys. Rev. B **72**, 115331 (2005).
[8] X. Hu and S. Das Sarma, Phys. Rev. Lett. **96**, 100501 (2006).
[9] P. Hawrylak and M. Korkusinski, Solid State Commun. **136**, 508 (2005).
[10] I. Puerto Gimenez, M. Korkusinski, and P. Hawrylak, Phys. Rev. B **76**, 075336 (2007).
[11] D. P. DiVincenzo, D. Bacon, J. Kempe, G. Burkard, and K. B. Whaley, Nature (London) **408**, 339 (2000).
[12] L. Gaudreau, S. A. Studenikin, A. S. Sachrajda, P. Zawadzki, A. Kam, J. Lapointe, M. Korkusinski, and P. Hawrylak, Phys. Rev. Lett. **97**, 036807 (2006).
[13] D. Schröer, A. D. Greentree, L. Gaudreau, K. Eberl, L. C. L. Hollenberg, J. P. Kotthaus, and S. Ludwig, Phys. Rev. B **76**, 075306 (2007).
[14] R.-B. Liu, W. Yao, and L. Sham, New J. Phys. **9**, 226 (2007).
[15] K. Roszak, A. Grodecka, P. Machnikowski, and T. Kuhn, Phys. Rev. B **71**, 195333 (2005).
[16] M. Korkusinski, I. P. Gimenez, P. Hawrylak, L. Gaudreau, S. A. Studenikin, and A. S. Sachrajda, Phys. Rev. B **75**, 115301 (2007).
[17] E. A. Laird, C. Barthel, E. I. Rashba, C. M. Marcus, M. P. Hanson, and A. C. Gossard, Phys. Rev. Lett. **99**, 246601 (2007).
[18] M. Pioro-Ladrière, Y. Tokura, T. Obata, T. Kubo, and S. Tarucha, Appl. Phys. Lett. **90**, 024105 (2007).
[19] F. Delgado, Y. P. Shim, M. Korkusinski, and P. Hawrylak, Phys. Rev. B **76**, 115332 (2007).
[20] V. Pokrovsky and N. Sinitsyn, Phys. Rev. B **69**, 104414 (2004).
[21] I. A. Merkulov, A. L. Efros, and M. Rosen, Phys. Rev. B **65**, 205309 (2002).
[22] J. M. Taylor, J. R. Petta, A. C. Johnson, A. Yacoby, C. M. Marcus, and M. D. Lukin, Phys. Rev. B **76**, 035315 (2007).
[23] J. R. Petta, A. C. Johnson, J. M. Taylor, E. A. Laird, A. Yacoby, M. D. Lukin, C. M. Marcus, M. P. Hanson, and A. C. Gossard, Science **309**, 2180 (2005).
[24] A. Greilich, D. R. Yakovlev, A. Shabaev, A. L. Efros, I. A. Yugova, R. Oulton, V. Stavarache, D. Reuter, A. Wieck, and M. Bayer, Science **313**, 341 (2006).